Accepted to the Astrophysical Journal Supplements: May 9, 2003
Preprint typeset using LaTeX style emulateapj v. 11/12/01

arXiv:astro-ph/0305313v1 16 May 2003

NEW DAMPED Lyα METALLICITIES FROM ESI SPECTROSCOPY OF FIVE PALOMAR SKY SURVEY QUASARS

JASON X. PROCHASKA
UCO/Lick Observatory
University of California, Santa Cruz; Santa Cruz, CA 95064

SANDRA CASTRO[1,2] & S. G. DJORGOVSKI[1]
Palomar Observatory, California Institute of Technology
MS 105-24; Pasadena, CA 91125
Accepted to the Astrophysical Journal Supplements: May 9, 2003

ABSTRACT

This paper presents chemical abundance measurements for 12 new $z > 3$ damped Lyα systems discovered toward five quasars from the Palomar Sky Survey. We determine H I column densities from profile fits to the observed damped Lyα profiles and measure ionic column densities and limits for all observed metal-line transitions. This dataset, acquired with the Echellette Spectrograph and Imager on the Keck II telescope, adds to the rapidly growing database of damped Lyα abundances. It will impact studies of chemical evolution in the early universe and help identify candidates for detailed follow-up observations with echelle spectrographs. We report the discovery of the first quasar sightline with four cosmologically distinct damped Lyα systems.

Subject headings: galaxies: abundances — galaxies: chemical evolution — quasars : absorption lines — nucleosynthesis

1. INTRODUCTION

Studies of absorption line systems in the spectra of high-redshift QSOs continue to provide valuable insights into the early chemical evolution of galaxies and IGM. One sample of bright ($r \lesssim 19.5$ mag), high-redshift ($z \sim 3.9 - 4.6$) QSOs is the sample discovered in Digital Palomar Observatory Sky Survey (DPOSS; Djorgovski et al. 1999, and in prep.). The QSOs were discovered using now standard color selection techniques; for more details, see, e.g., Kennefick et al. 1995a, 1995b, or Djorgovski et al. 2001. The sample (commonly designated as PSS, for Palomar Sky Survey), including many as yet unpublished objects, is available on line[3].

Relatively high–resolution, high-S/N ($R \approx 4500$, S/N $>$ 15 per 10km/s pixel) spectra of nearly all PSS QSOs and a number of additional bright, high-z QSOs from other surveys, were obtained using the ESI instrument (Sheinis et al. 2002) at the Keck II 10-m telescope in the course of a survey for high column density absorbers. The results of this survey will be presented in future papers (Castro et al. 2003, Djorgovski et al. , in prep.). This paper serves as a companion to the ESI/Keck II Damped Lyα Abundance Database comprised by Prochaska et al. (2003; hereafter P03). Here we present the chemical abundance measurements from the PSS damped Lyα sample avoiding repetition with the results presented in P03. We analyse 12 damped Lyα systems toward 5 quasars. This incidence of damped Lyα systems is higher than a random sample because we have restricted the analysis to sightlines showing at least one DLA. Even still, the incidence is higher than expected from the number density of DLA in the literature (e.g. Storrie-Lombardi and Wolfe 2000) perhaps owing to the higher resolution of our spectra but more likely small number statistics. We present the relevant figures and tables related to our abundance analysis and withhold extensive analysis to future papers. This paper is outlined as follows. We describe the observations and data reduction routines in § 2. The individual damped Lyα systems are presented in § 3 and § 4 provides a brief summary.

[1] Visiting Astronomer, W.M. Keck Telescope. The Keck Observatory is a joint facility of the University of California, California Institute of Technology, and NASA.

[2] Current address: Infrared Processing and Analysis Center, 100-22, California Institute of Technology, Pasadena, CA, 91125

[3] `http://www.astro.caltech.edu/~george/z4.qsos`

Table 1
JOURNAL OF OBSERVATIONS

Quasar	R	z_{em}	Date	Exp (s)	Arcs
PSS0007+2417	18.7	4.05	06sep00	3600	CuAr
PSS1535+2943	18.9	3.99	15may00	5400	CuAr+Xe
PSS1715+3809	18.6	4.52	03sep00	3600	CuAr
PSS1802+5616	19.2	4.18	05sep00	5400	CuAr
PSS2315+0921	19.5	4.30	05sep00	5400	CuAr

Table 2
IONIC COLUMN DENSITIES: PSS0007+2417, $z = 3.496$

Ion	λ	AODM	$N_{\rm adopt}$	[X/H]
Al II	1670.8	> 13.249	> 13.249	> -2.341
Al III	1854.7	12.694 ± 0.052		
Al III	1862.8	12.696 ± 0.086		
Si II	1526.7	> 14.520	15.077 ± 0.040	-1.583 ± 0.108
Si II	1808.0	15.077 ± 0.040		
Fe II	1608.5	> 14.630	> 14.630	> -1.970
Fe II	1611.2	< 15.262		
Ni II	1370.1	13.518 ± 0.040	13.529 ± 0.036	-1.821 ± 0.106
Ni II	1741.6	< 13.842		
Ni II	1751.9	13.591 ± 0.081		
Zn II	2062.7	< 12.390	< 12.390	< -1.380

2. OBSERVATIONS, DATA REDUCTION AND ANALYSIS

With the commissioning of the Echellette Spectrograph and Imager, the DPOSS team (PI: Djorgovski) initiated

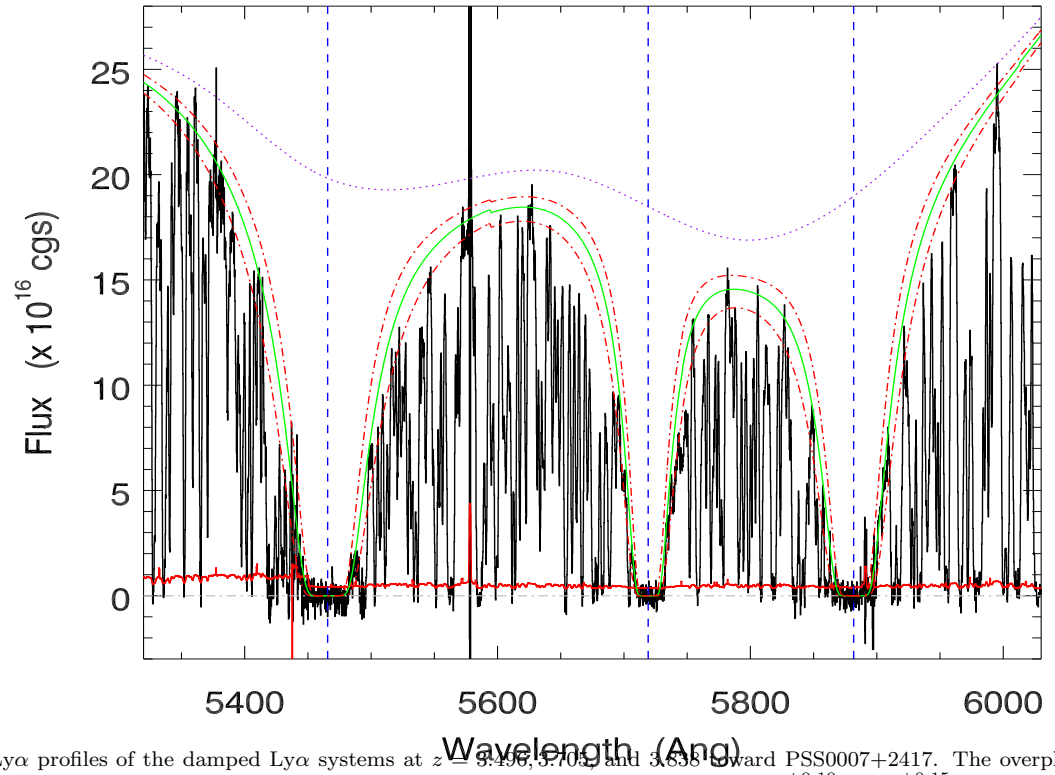

FIG. 1.— Lyα profiles of the damped Lyα systems at $z = 3.496, 3.705$, and 3.838 toward PSS0007+2417. The overplotted solid line and accompanying dash-dot lines trace the best fit solutions corresponding to $\log N(\mathrm{HI}) = 21.10^{+0.10}_{-0.10}, 20.55^{+0.15}_{-0.15}$ and $20.85^{+0.15}_{-0.15}$. The solution for all three damped Lyα systems are reasonably well constrained by both the wings and cores of the profiles. One notes that the predicted continuum exhibits significant variation, primarily due to the presence of the Lyα and O VI emission peaks. Because the continuum is more poorly constrained from 5600–6000Å, we report 0.15 dex uncertainties for the two higher redshift DLA.

TABLE 3
IONIC COLUMN DENSITIES: PSS0007+2417, $z = 3.705$

Ion	λ	AODM	N_{adopt}	[X/H]
C II	1334.5	> 14.530	> 14.530	> -2.610
C II*	1335.7	13.242 ± 0.061		
C IV	1548.2	13.460 ± 0.031		
O I	1302.2	> 14.855	> 14.855	> -2.435
Al II	1670.8	> 12.895	> 12.895	> -2.145
Si II	1304.4	> 14.372	> 14.372	> -1.738
Si II	1526.7	> 14.291		
Si II	1808.0	< 14.854		
Si IV	1393.8	13.329 ± 0.019		
Si IV	1402.8	13.433 ± 0.032		
Fe II	1608.5	> 14.211	> 14.211	> -1.839
Fe II	1611.2	< 14.603		
Ni II	1370.1	< 13.612	< 13.197	< -1.603
Ni II	1709.6	< 13.311		
Ni II	1751.9	< 13.507		

TABLE 4
IONIC COLUMN DENSITIES: PSS0007+2417, $z = 3.838$

Ion	λ	AODM	N_{adopt}	[X/H]
C II	1334.5	> 14.394	> 14.394	> -3.046
C II*	1335.7	< 12.891		
C IV	1548.2	13.579 ± 0.024		
C IV	1550.8	13.614 ± 0.037		
O I	1302.2	> 14.643	> 14.643	> -2.947
Al II	1670.8	12.699 ± 0.018	12.699 ± 0.019	-2.641 ± 0.151
Si II	1526.7	> 14.006	> 14.006	> -2.404
Si II	1808.0	< 14.441		
Si IV	1393.8	12.962 ± 0.035		
Fe II	1608.5	13.906 ± 0.031	13.906 ± 0.031	-2.444 ± 0.153
Ni II	1317.2	< 13.042	< 13.042	< -2.058
Ni II	1741.6	< 13.234		
Ni II	1751.9	< 13.399		

an observing campaign to survey $z > 3$ damped Lyα systems. A full account of this survey will be presented in a future paper. In Table 1 we present a journal of the observations for the background quasars of the damped Lyα systems presented in this paper. Column 1 gives the name, column 2 is the apparent R magnitude of the quasar, column 3 is the emission redshift, column 4 gives the date of the observation, column 5 is the exposure time, and column 6 lists the arc calibrations available for data reduction. To avoid repetition, we have restricted the sample analysed here to the sub-set which were not analysed by P03. The P03 survey has comparable S/N data but higher resolution ($R \approx 9000$) and therefore more accurate abundance measurements.

Data reduction was performed using the ESI/IDL package built by Prochaska (P03). In contrast to the P03 database, the majority of observations presented here were calibrated with the CuAr lamps only. This limits the spectral coverage to $\lambda < 9000$Å due to a steep drop in trans-

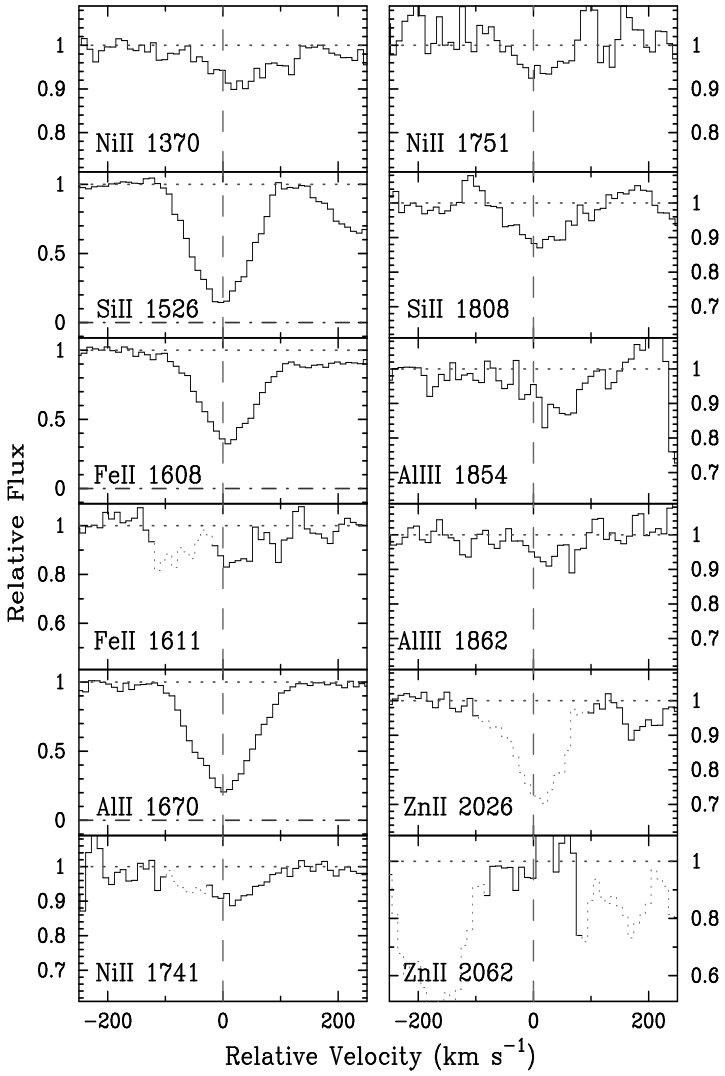

FIG. 2.— Velocity plot of the metal-line transitions for the damped Lyα system at $z = 3.496$ toward PSS0007+2417. The vertical line at $v = 0$ corresponds to $z = 3.4962$.

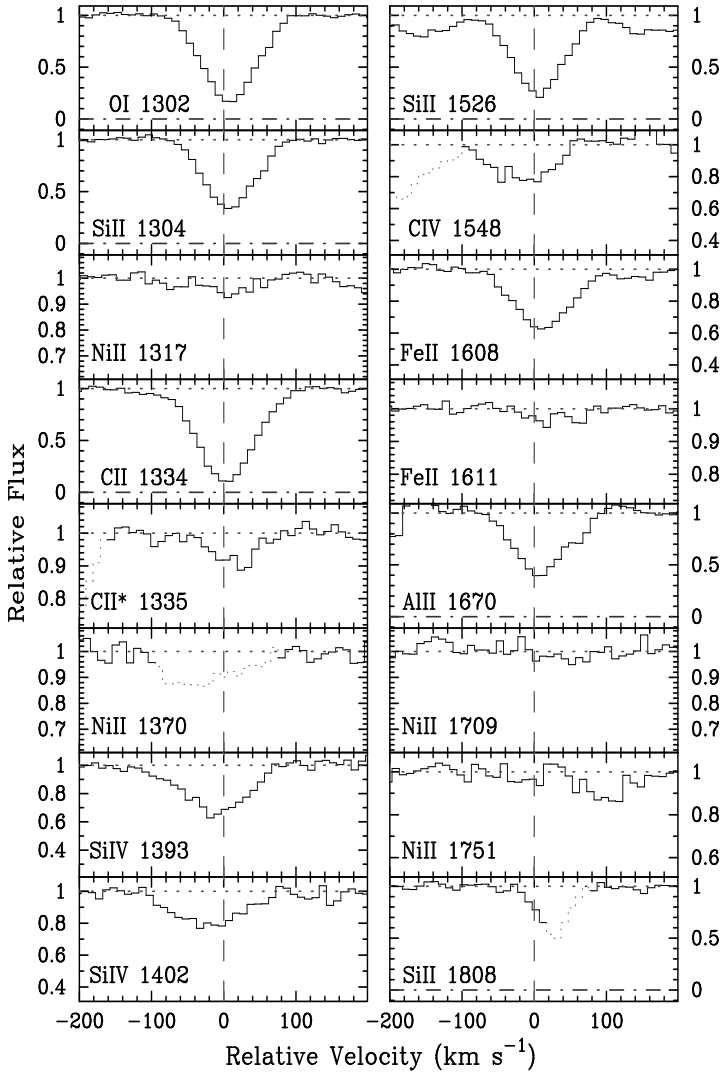

FIG. 3.— Velocity plot of the metal-line transitions for the damped Lyα system at $z = 3.705$ toward PSS0007+2417. The vertical line at $v = 0$ corresponds to $z = 3.70454$.

missivity of the fibers which feed the CuAr lamps to the spectrograph. The other major difference in the datasets is that all of the data were taken with the $1.0''$ slit (the majority of data in P03 used the $0.5''$ slit). Both the lower resolution and the limited arc calibration frames imply poorer sky line subtraction at $\lambda > 6000$Å. Nevertheless, the spectra provide multiple metal-line transitions for most of the damped Lyα systems considered here and reasonably accurate abundance measurements. In the future, however, we may implement a reduction scheme using the night sky lines to better calibrate the reddest orders of the spectra.

Measurements of H I column densities N(HI) and ionic column densities were determined using the techniques described in P03. Specifically, we performed Voigt profile fits to the Lyα transitions and utilized the apparent optical depth method (Savage and Sembach 1991) to evaluate column densities of unsaturated, unblended metal-line transitions. Because the Lyα profiles extend many angstroms of spectra, the lower resolution of this dataset in comparison with P03 implies a minimal difference in N(HI) precision. While our H I analysis is not based on a χ^2 minimization technique, we report conservative statistical errors which we contend correspond to 95%c.l. (see P03 for a complete discussion). For the ionic column densities, we have taken greater care to account for the effects of line-saturation. In general, we have been very conservative in our analysis, reporting lower limits in those cases where line-saturation is possible. Generally, this included all profiles where the peak optical depth of any 10 km s^{-1} pixel exceeds 0.5 (i.e. normalized flux less than 60% the quasar continuum). Finally although we report formal statistical errors from our analysis of the ionic column densities, we caution that the systematic effects of line-saturation and continuum placement will lend larger uncertainties in most cases. We rec-

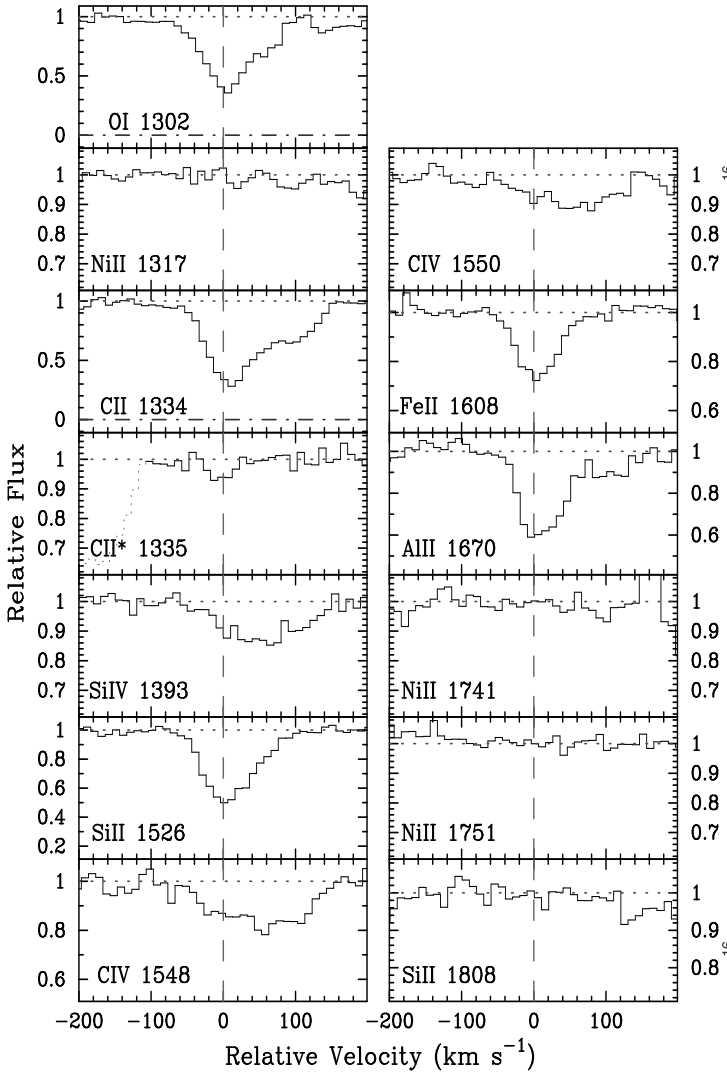

FIG. 4.— Velocity plot of the metal-line transitions for the damped Lyα system at $z = 3.838$ toward PSS0007+2417. The vertical line at $v = 0$ corresponds to $z = 3.83823$.

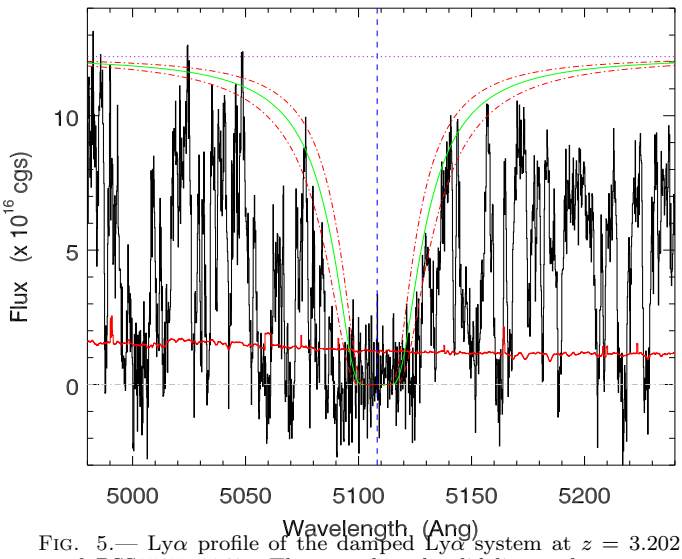

FIG. 5.— Lyα profile of the damped Lyα system at $z = 3.202$ toward PSS1535+2943. The overplotted solid line and accompanying dash-dot lines trace the best fit solution corresponding to $\log N(\mathrm{HI}) = 20.65^{+0.15}_{-0.15}$. Although the quasar continuum is well determined across this region of the spectrum, the core of this Lyα profile is not well sampled and we assign an uncertainty of 0.15 dex.

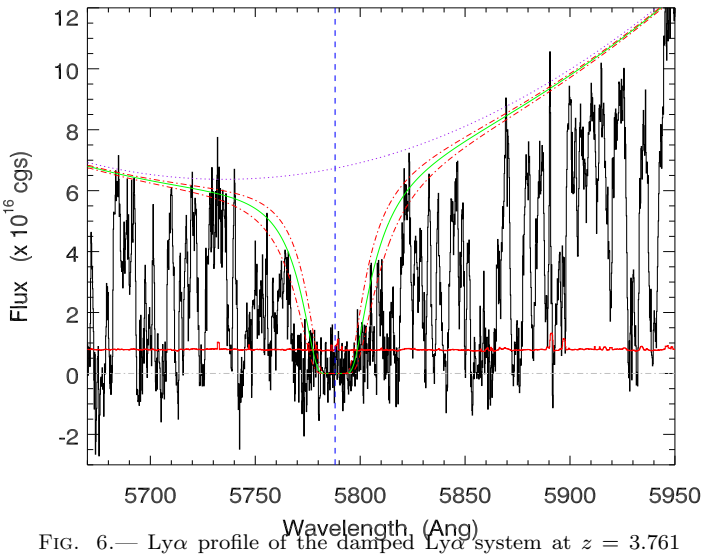

FIG. 6.— Lyα profile of the damped Lyα system at $z = 3.761$ toward PSS1535+2943. The overplotted solid line and accompanying dash-dot lines trace the best fit solution corresponding to $\log N(\mathrm{HI}) = 20.40^{+0.15}_{-0.15}$.

ommend that the reader assume 1σ uncertainties of at least 0.1 dex for all measurements.

Throughout the paper, we adopt the wavelengths and oscillator strengths presented in Table 2 of P03. We also adopt solar meteoritic abundances from Grevesse et al. (1996) and Holweger (2001) for the elemental abundances listed in the paper.

3. INDIVIDUAL SYSTEMS

In this section we present the metal-line and Lyα profiles of the DLA and tabulate the measured ionic column densities. For the metal-line transitions, we integrated unblended velocity profiles over a velocity region including all significant absorption. The exact values can be obtained from the authors upon request. Regarding the figures, $v = 0$ km s^{-1} is arbitrarily defined and blends from coincident absorption lines are indicated by dotted lines. For the low-ion transitions – the dominant ionic transition of a given element in an H I region – we tabulate N_{adopt} by taking the weighted mean (or limit) of all measured transitions. For these cases, we also convert N_{adopt} into an elemental abundance [X/H] assuming no ionization corrections and adopting solar meteoritic abundances.

3.1. *PSS0007+2417,* $z = 3.496, 3.705, 3.838$

This quasar exhibits three damped Lyα systems along its sightline whose Lyα profiles are shown together in Figure 1. The N(HI) values are reasonably well constrained

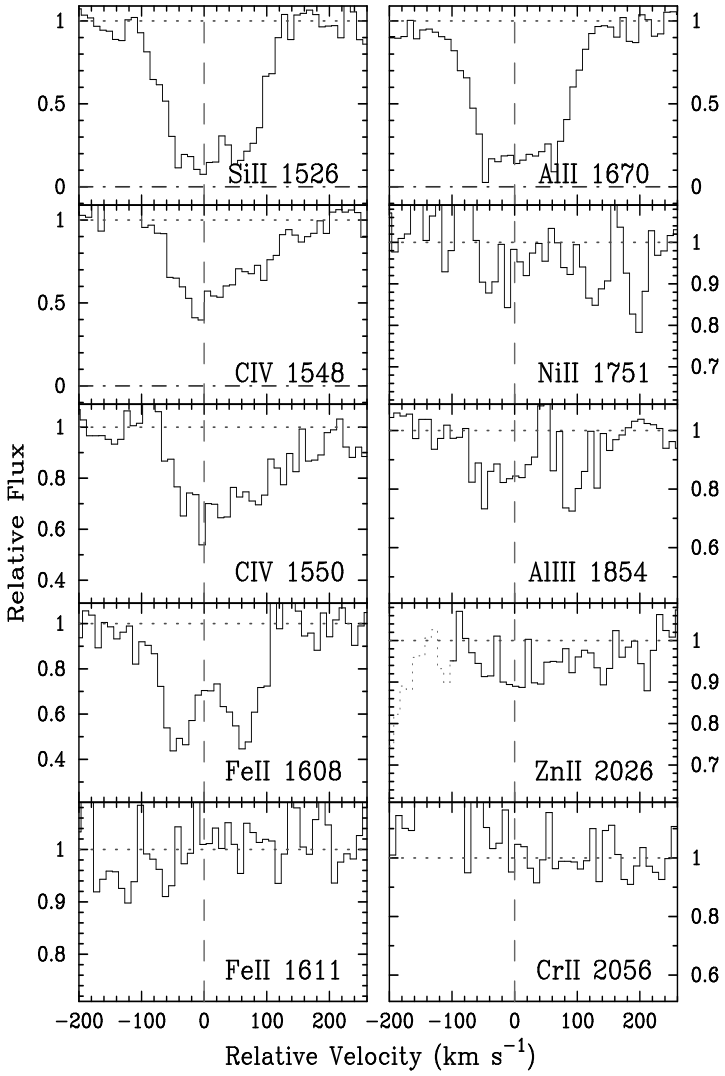

FIG. 7.— Velocity plot of the metal-line transitions for the damped Lyα system at $z = 3.202$ toward PSS1535+2943. The vertical line at $v = 0$ corresponds to $z = 3.2020$.

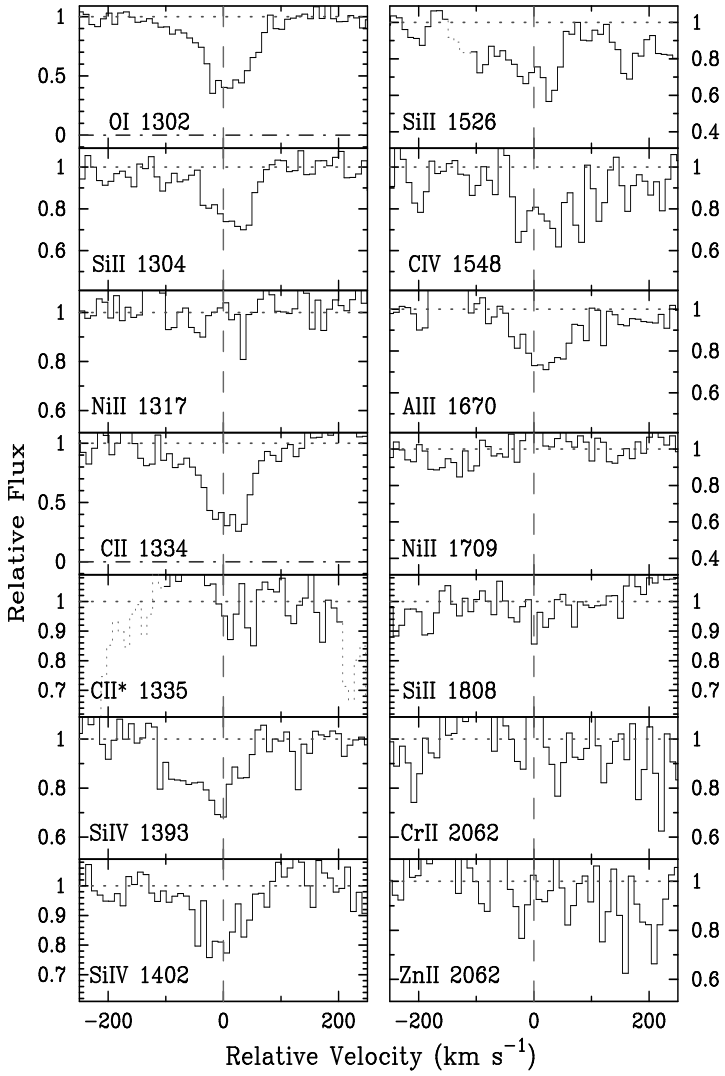

FIG. 8.— Velocity plot of the metal-line transitions for the damped Lyα system at $z = 3.761$ toward PSS1535+2943. The vertical line at $v = 0$ corresponds to $z = 3.7612$.

TABLE 5
IONIC COLUMN DENSITIES: PSS1535+2943, $z = 3.202$

Ion	λ	AODM	$N_{\rm adopt}$	[X/H]
C IV	1548.2	< 14.085		
C IV	1550.8	14.232 ± 0.040		
Al II	1670.8	> 13.560	> 13.560	> -1.580
Al III	1854.7	12.848 ± 0.095		
Si II	1526.7	> 14.742	> 14.742	> -1.468
Cr II	2056.3	< 13.189	< 13.189	< -1.131
Fe II	1608.5	> 14.603	> 14.603	> -1.547
Fe II	1611.2	< 15.198		
Ni II	1751.9	< 13.972	< 13.972	< -0.928
Zn II	2026.1	< 12.531	< 12.531	< -0.789

TABLE 6
IONIC COLUMN DENSITIES: PSS1535+2943, $z = 3.761$

Ion	λ	AODM	$N_{\rm adopt}$	[X/H]
C II	1334.5	> 14.369	> 14.369	> -2.621
C II*	1335.7	< 13.291		
C IV	1548.2	13.712 ± 0.079		
O I	1302.2	> 14.711	> 14.711	> -2.429
Al II	1670.8	12.563 ± 0.051	12.563 ± 0.051	-2.327 ± 0.158
Si II	1304.4	13.940 ± 0.048	13.940 ± 0.049	-2.020 ± 0.158
Si II	1526.7	13.970 ± 0.040		
Si II	1808.0	< 14.819		
Si IV	1393.8	13.242 ± 0.064		
Si IV	1402.8	13.356 ± 0.085		
Ni II	1317.2	< 13.453	< 13.453	< -1.197
Ni II	1709.6	< 13.690		

although the proximity of the DLA and the presence of the O VI and Lyα emission peaks do complicate the con-

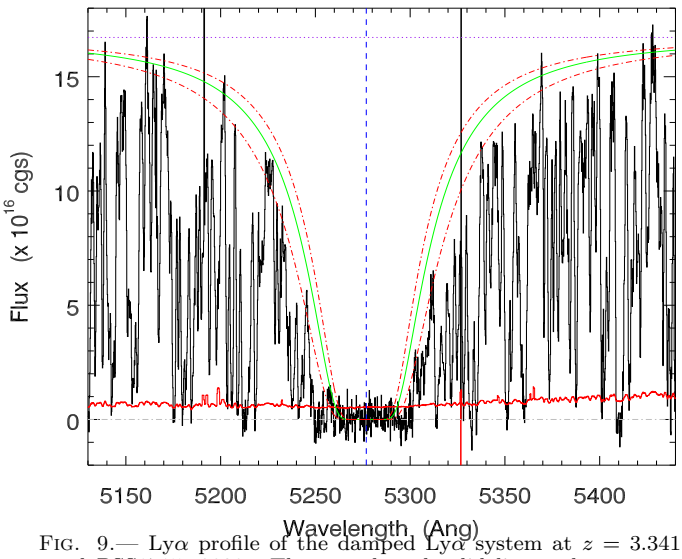

FIG. 9.— Lyα profile of the damped Lyα system at $z = 3.341$ toward PSS1715+3809. The overplotted solid line and accompanying dash-dot lines trace the best fit solution corresponding to $\log N(\mathrm{HI}) = 21.05^{+0.15}_{-0.10}$. Although it may appear from the figure that we have underestimated the N(HI) value, the flux at $\lambda \approx 5260$Å is significant and the continuum is well constrained. Together, these data imply the value we have adopted.

TABLE 7
IONIC COLUMN DENSITIES: PSS1715+3809, $z = 3.341$

Ion	λ	AODM	N_{adopt}	[X/H]
Al II	1670.8	12.551 ± 0.021	12.551 ± 0.021	-2.989 ± 0.127
Al III	1854.7	< 12.325		
Si II	1808.0	< 14.488	< 14.488	< -2.122
Cr II	2056.3	< 12.773	< 12.773	< -1.947
Fe II	1608.5	13.743 ± 0.039	13.743 ± 0.039	-2.807 ± 0.131
Fe II	1611.2	< 14.699		
Ni II	1741.6	< 13.294	< 13.294	< -2.006
Zn II	2026.1	< 12.113	< 12.113	< -1.607

tinuum placement. All three DLA exhibit a significant number of metal-line transitions (Figures 2-4) and have reasonably well determined, low metallicities. The ionic column densities and elemental abundances are listed in Tables 2-4.

TABLE 8
IONIC COLUMN DENSITIES: PSS1802+5616, $z = 3.391$

Ion	λ	AODM	N_{adopt}	[X/H]
C IV	1548.2	13.990 ± 0.026		
C IV	1550.8	14.115 ± 0.037		
Al II	1670.8	> 13.152	> 13.152	> -1.638
Al III	1854.7	< 12.441		
Si II	1526.7	> 14.314	> 14.314	> -1.546
Si II	1808.0	< 14.556		
Fe II	1608.5	14.256 ± 0.037	14.256 ± 0.037	-1.544 ± 0.107
Ni II	1709.6	< 13.654	< 13.654	< -0.896
Ni II	1751.9	< 13.717		
Zn II	2026.1	< 12.405	< 12.405	< -0.565

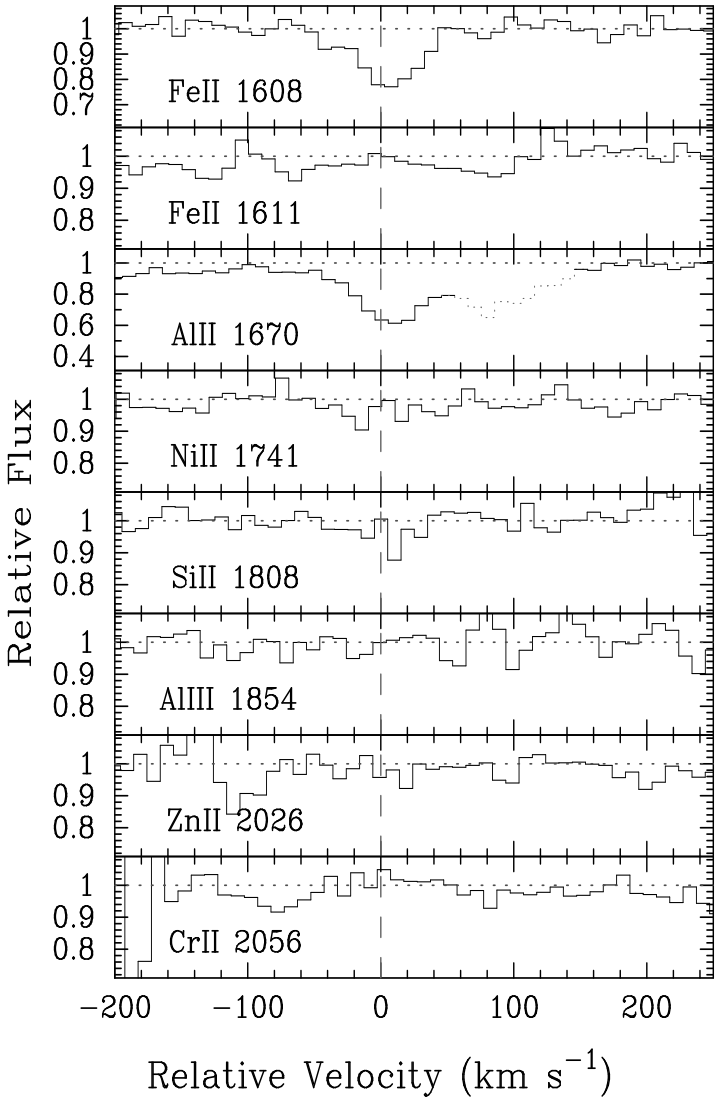

FIG. 10.— Velocity plot of the metal-line transitions for the damped Lyα system at $z = 3.341$ toward PSS1715+3809. The vertical line at $v = 0$ corresponds to $z = 3.3407$.

TABLE 9
IONIC COLUMN DENSITIES: PSS1802+5616, $z = 3.554$

Ion	λ	AODM	N_{adopt}	[X/H]
C IV	1548.2	13.820 ± 0.036		
C IV	1550.8	14.063 ± 0.039		
Al III	1854.7	< 12.496		
Si II	1526.7	> 14.239	> 14.239	> -1.821
Si II	1808.0	< 15.122		
Si IV	1393.8	13.587 ± 0.012		
Si IV	1402.8	13.664 ± 0.020		
Fe II	1608.5	14.075 ± 0.061	14.075 ± 0.061	-1.925 ± 0.117
Ni II	1741.6	< 13.299	< 13.299	< -1.451
Zn II	2026.1	< 12.632	< 12.632	< -0.538

3.2. *PSS1535+2943*, $z = 3.202, 3.761$

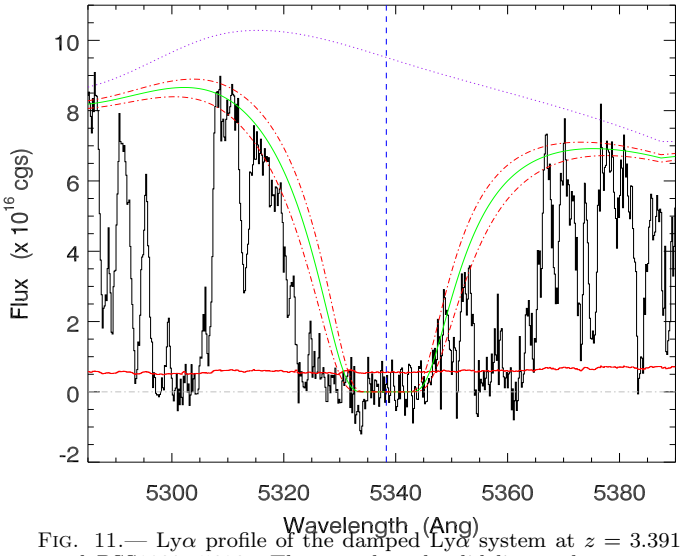

FIG. 11.— Lyα profile of the damped Lyα system at $z = 3.391$ toward PSS1802+5616. The overplotted solid line and accompanying dash-dot lines trace the best fit solution corresponding to $\log N(\mathrm{HI}) = 20.30^{+0.10}_{-0.10}$. This damped system just satisfies the DLA criterion of $2 \times 10^{20}\,\mathrm{cm}^{-2}$. Although the fit to the Lyα profile is complicated by the O VI emission peak, the N(HI) value is well constrained by the wings of the profile.

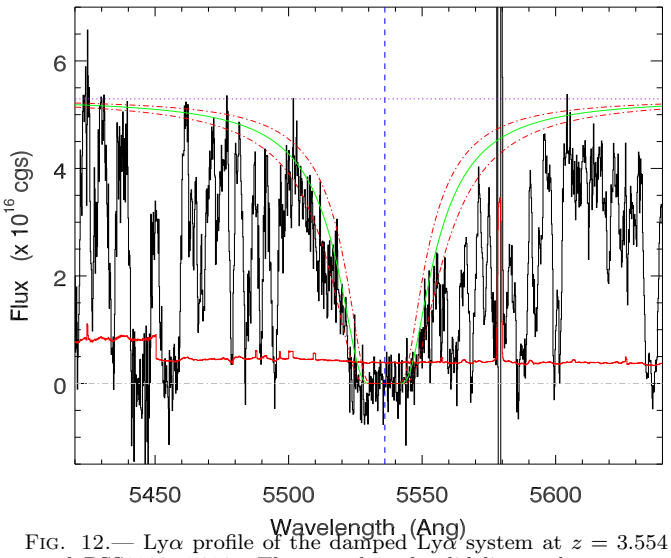

FIG. 12.— Lyα profile of the damped Lyα system at $z = 3.554$ toward PSS1802+5616. The overplotted solid line and accompanying dash-dot lines trace the best fit solution corresponding to $\log N(\mathrm{HI}) = 20.50^{+0.10}_{-0.10}$.

The Lyα profiles for the two damped systems along this sightline are displayed in Figures 5 and 6 and they provide reasonably good measurements of N(HI) for each system. The damped system at $z = 3.202$ exhibits only a few metal-line transitions outside the Lyα forest and the majority of these are saturated (Figure 7). Nevertheless, a reasonable estimate of the Fe metallicity can be determined from the competing upper and lower limits (Fe II 1608, 1611; Table 5). Regarding the DLA at $z = 3.761$, its Fe II transitions are lost in the thick band of atmospheric absorption at $\lambda \approx 7650$Å but the system exhibits unsaturated Si II and Al II profiles which provide accurate metal abundances (Figure 8, Table 6).

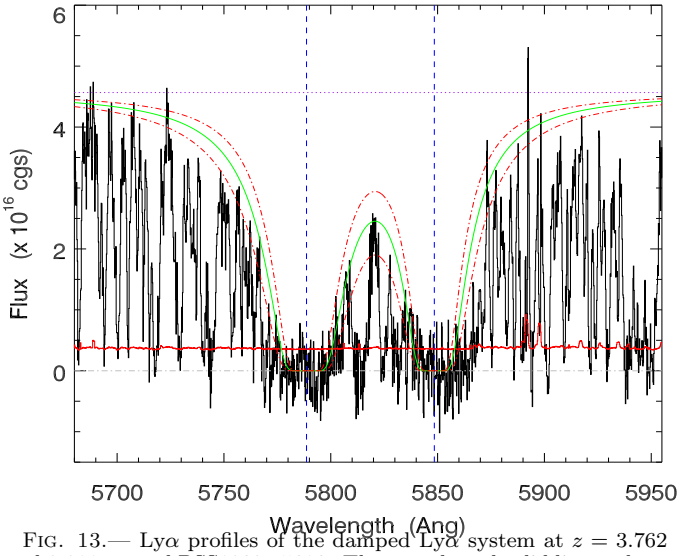

FIG. 13.— Lyα profiles of the damped Lyα system at $z = 3.762$ and 3.811 toward PSS1802+5616. The overplotted solid line and accompanying dash-dot lines trace the best fit solution corresponding to $\log N(\mathrm{HI}) = 20.55^{+0.15}_{-0.15}$ and $20.35^{+0.20}_{-0.20}$ respectively. The proximity of the two DLA complicates the solution and we report N(HI) values with lower precision. In particular, there is little data outside of $\lambda \approx 5820$Å constraining the $z = 3.811$ DLA.

TABLE 10
IONIC COLUMN DENSITIES: PSS1802+5616, $z = 3.762$

Ion	λ	AODM	N_{adopt}	[X/H]
C II	1334.5	> 14.674	> 14.674	> -2.466
C II*	1335.7	< 12.853		
C IV	1550.8	< 13.374		
Al II	1670.8	> 12.960	> 12.960	> -2.080
Si II	1526.7	> 14.370	> 14.370	> -1.740
Si II	1808.0	< 14.747		
Ni II	1370.1	< 13.332	< 13.332	< -1.468
Ni II	1709.6	< 13.620		

TABLE 11
IONIC COLUMN DENSITIES: PSS1802+5616, $z = 3.811$

Ion	λ	AODM	N_{adopt}	[X/H]
C II	1334.5	> 14.412	> 14.412	> -2.528
C II*	1335.7	< 12.978		
C IV	1548.2	13.407 ± 0.079		
C IV	1550.8	< 13.393		
Al II	1670.8	12.393 ± 0.045	12.393 ± 0.045	-2.447 ± 0.205
Si II	1526.7	13.870 ± 0.102	13.870 ± 0.102	-2.040 ± 0.225
Si II	1808.0	< 14.808		
Fe II	1608.5	13.665 ± 0.104	13.665 ± 0.104	-2.185 ± 0.225
Ni II	1317.2	< 13.078	< 13.078	< -1.522
Ni II	1370.1	< 13.411		
Ni II	1741.6	< 13.577		

3.3. *PSS1715+3809, $z = 3.341$*

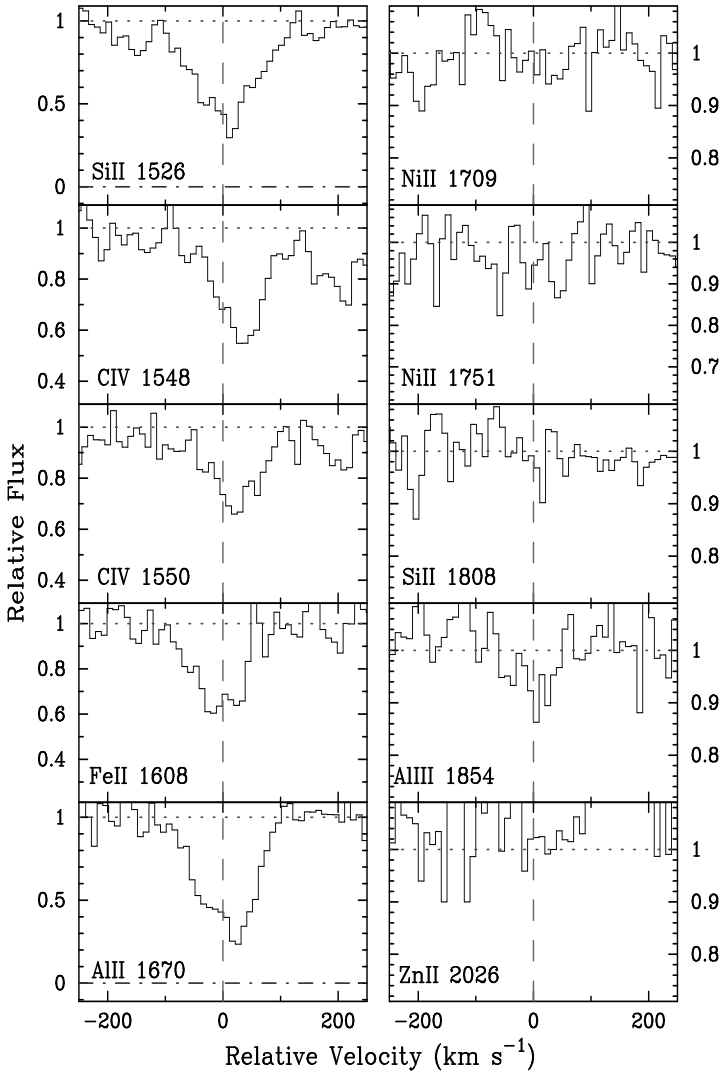

FIG. 14.— Velocity plot of the metal-line transitions for the damped Lyα system at $z = 3.391$ toward PSS1802+5616. The vertical line at $v = 0$ corresponds to $z = 3.39126$.

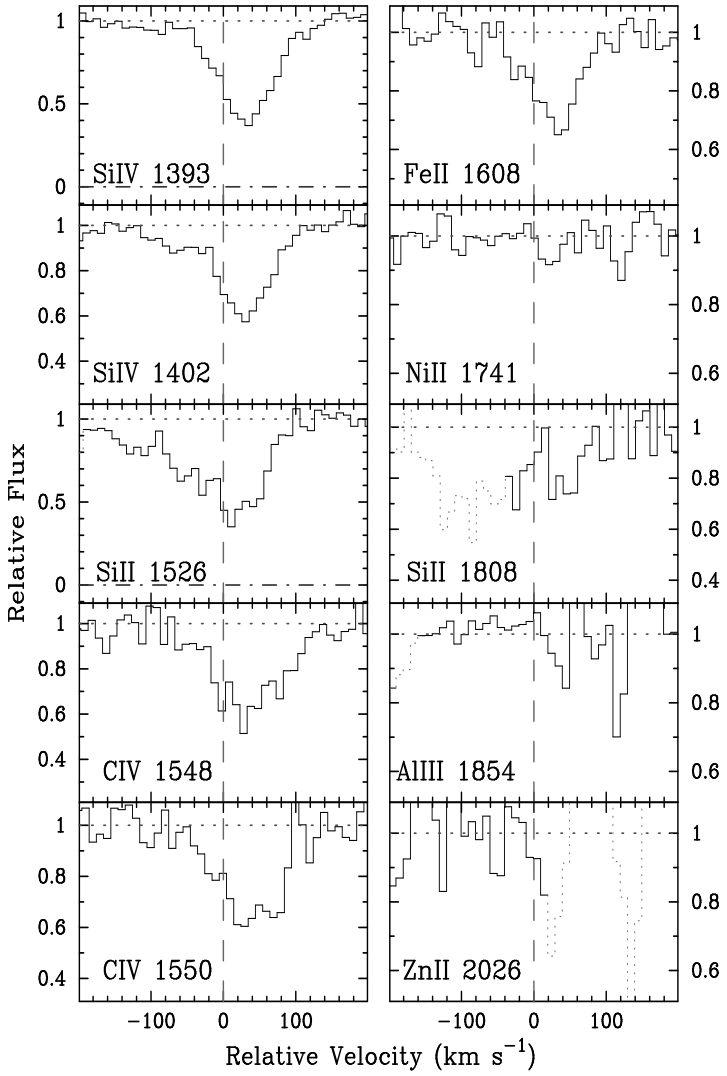

FIG. 15.— Velocity plot of the metal-line transitions for the damped Lyα system at $z = 3.554$ toward PSS1802+5616. The vertical line at $v = 0$ corresponds to $z = 3.5539$.

This is the only quasar reported here with a single damped Lyα system. Its Lyα profile and corresponding metal-lines are presented in Figures 9 and 10. This damped system is well separated from the emission redshift of the quasar and therefore exhibits few metal-line transitions outside the Lyα forest. Nevertheless, the Fe II 1608 and Al II 1670 profiles indicate it possesses one of the lowest metallicities to date. Table 7 lists the values and limits measured for this DLA.

3.4. *PSS1802+5616,* $z = 3.391, 3.554, 3.762, 3.811$

This sightline marks the first quasar with four foreground damped Lyα systems. The Lyα profiles are plotted in Figures 11-13 and with the exception of the pair of DLA at $z \sim 3.8$, the N(HI) values are well constrained. The proximity of the pair and the poor sampling of the core of the Lyα profiles yield less constrained H I column densities. The metal-line transitions for the four DLA are presented in Figures 14-17. The systems exhibit rather similar metallicity, [M/H] ≈ -1.8, and are otherwise unremarkable (Tables 8-11).

TABLE 12
IONIC COLUMN DENSITIES: PSS2315+0921, $z = 3.219$

Ion	λ	AODM	$N_{\rm adopt}$	[X/H]
Al II	1670.8	> 13.240	> 13.240	> -2.600
Al III	1854.7	< 12.284		
Cr II	2056.3	< 13.191	< 13.191	< -1.829
Fe II	1608.5	> 14.557	> 14.557	> -2.293
Fe II	1611.2	< 14.983		
Zn II	2026.1	< 11.947	< 11.947	< -2.073

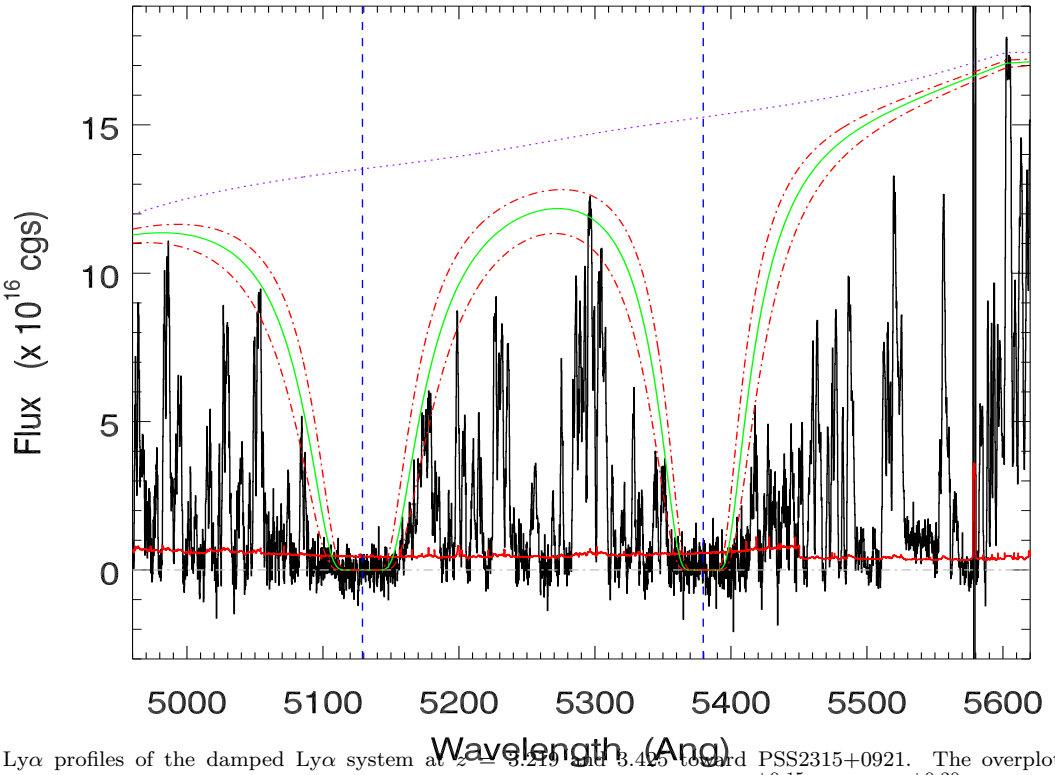

FIG. 18.— Lyα profiles of the damped Lyα system at $z = 3.219$ and 3.425 toward PSS2315+0921. The overplotted solid line and accompanying dash-dot lines trace the best fit solution corresponding to $\log N(\mathrm{HI}) = 21.35^{+0.15}_{-0.15}$ and $21.10^{+0.20}_{-0.20}$ respectively. The proximity of the two DLA complicates the solution and the quasar continuum is rapidly changing across this spectrum in part due to a higher redshift Lyman limit system. Finally, the metal-lines for the $z = 3.425$ DLA are very extended in velocity space, further complicating the N(HI) fit. Here we have assumed a single component which we found gives a comparable total N(HI) as a multi-component fit. Nevertheless, we attribute a 0.2 dex uncertainty to this measurement.

TABLE 13
IONIC COLUMN DENSITIES: PSS2315+0921, $z = 3.425$

Ion	λ	AODM	$N_{\rm adopt}$	[X/H]
C IV	1548.2	> 15.087		
C IV	1550.8	> 14.989		
Al II	1670.8	> 13.781	> 13.781	> -1.809
Si II	1526.7	> 15.016	15.149 ± 0.049	-1.511 ± 0.206
Si II	1808.0	15.149 ± 0.049		
Fe II	1608.5	> 14.635	> 14.635	> -1.965
Fe II	1611.2	< 14.979		
Ni II	1709.6	< 13.359	< 13.359	< -1.991
Ni II	1741.6	< 13.491		

3.5. *PSS2315+0921*, $z = 3.219, 3.425$

The two damped Lyα systems along this sightline exhibit H I column densities in excess of $10^{21}\,\mathrm{cm}^{-2}$ (Figure 18) and the largest in this sample. Examining the metal-line transitions for the two DLA (Figures 19,20) one notes significant differences. Specifically, the DLA at $z = 3.219$ is relatively metal-poor and shows very simple kinematics. In contrast, the DLA at $z = 3.425$ has metal-profiles extending ≈ 1000 km s^{-1}, one of the largest velocity fields exhibited by a DLA to date. Even a 90% optical-depth determined velocity width (Prochaska & Wolfe 1997) would exceed 400 km s^{-1} . Tables 12 and 13 list the column densities for these two galaxies.

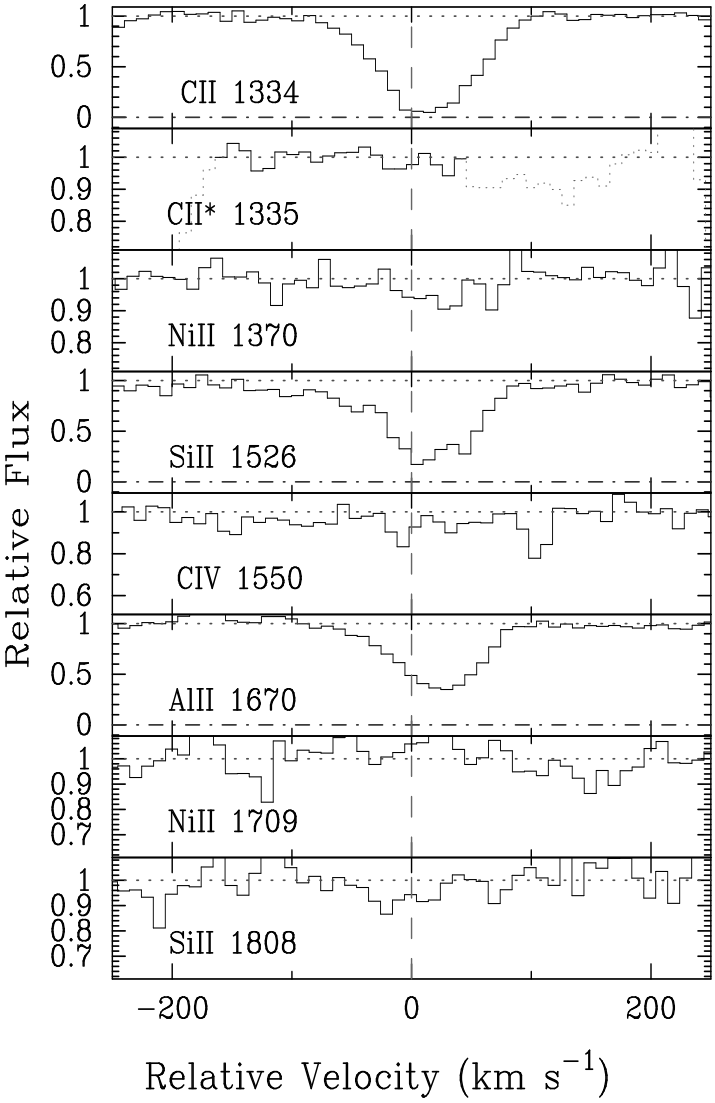

FIG. 16.— Velocity plot of the metal-line transitions for the damped Lyα system at $z = 3.762$ toward PSS1802+5616. The vertical line at $v = 0$ corresponds to $z = 3.7617$.

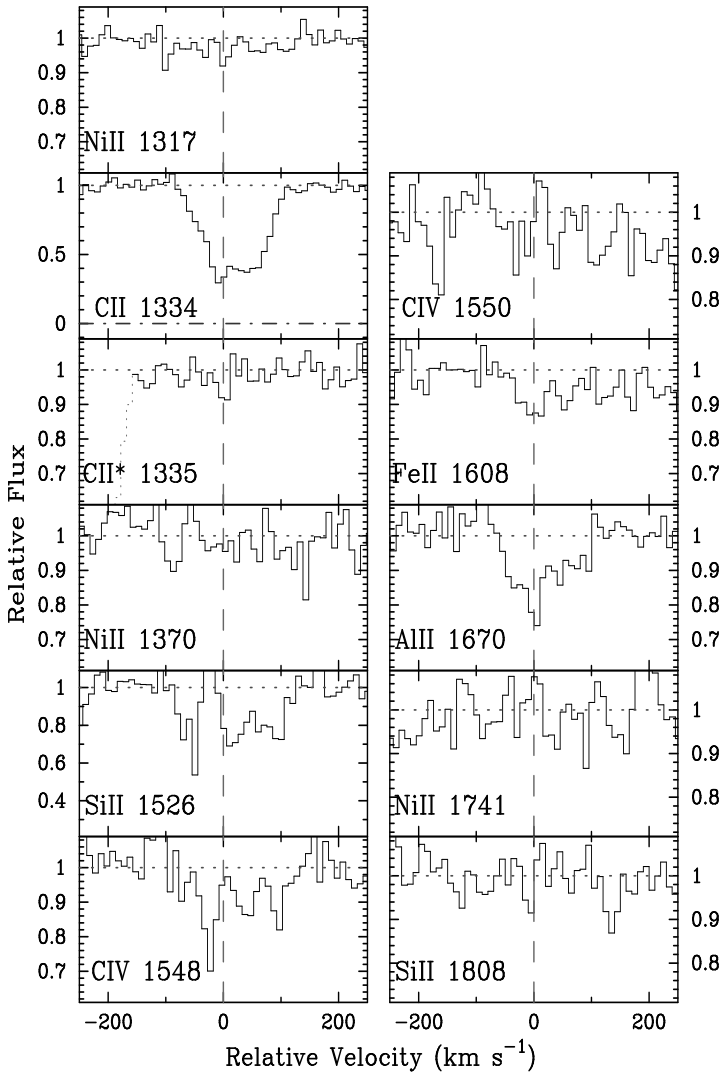

FIG. 17.— Velocity plot of the metal-line transitions for the damped Lyα system at $z = 3.811$ toward PSS1802+5616. The vertical line at $v = 0$ corresponds to $z = 3.8109$.

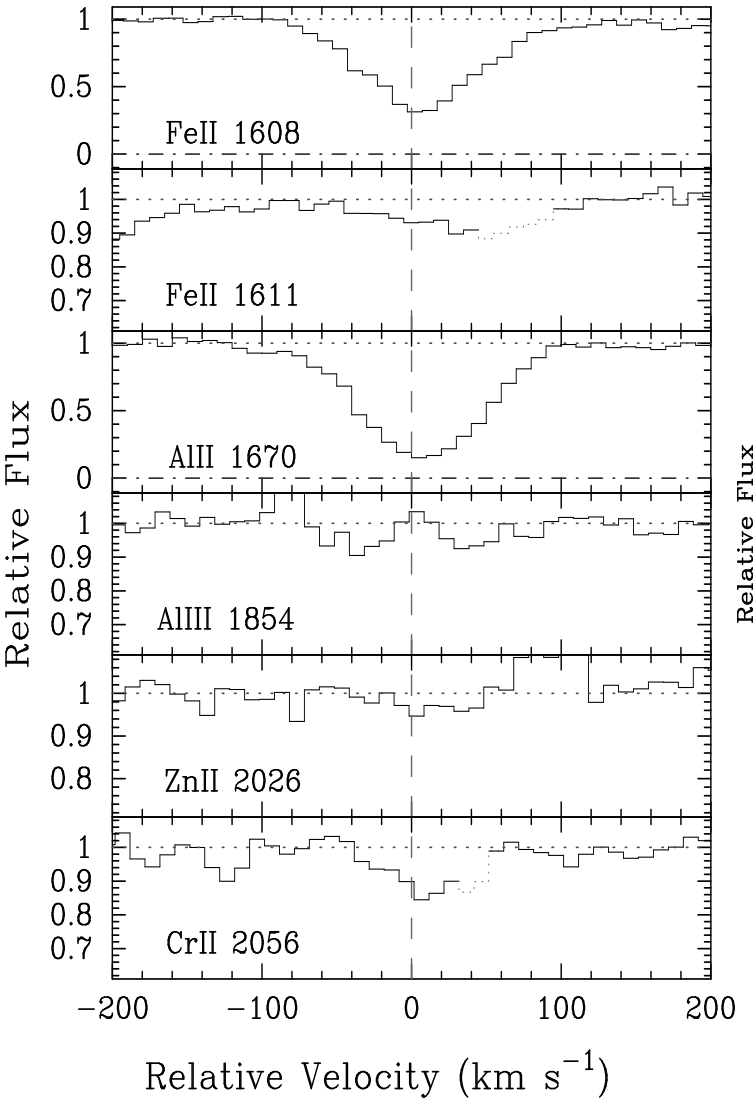

FIG. 19.— Velocity plot of the metal-line transitions for the damped Lyα system at $z = 3.219$ toward PSS2315+0921. The vertical line at $v = 0$ corresponds to $z = 3.2191$.

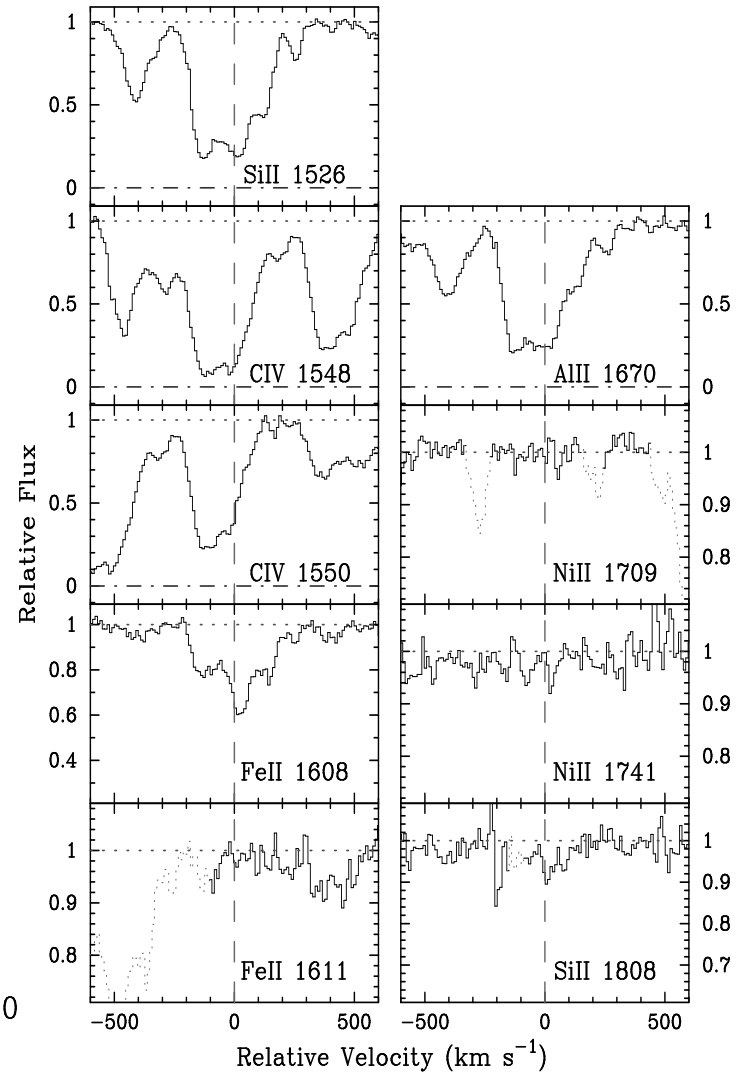

FIG. 20.— Velocity plot of the metal-line transitions for the damped Lyα system at $z = 3.425$ toward PSS2315+0921. The vertical line at $v = 0$ corresponds to $z = 3.4252$.

TABLE 14
ABUNDANCE SUMMARY

Name	z_{abs}	N(HI)	[C/H]	[O/H]	[Al/H]	[Si/H]	[Cr/H]	[Fe/H]	[Ni/H]	[Zn/H]
PSS0007+2417	3.496	21.10			> -2.341	-1.583	< -0.574	> -1.970	-1.821	< -1.380
PSS0007+2417	3.705	20.55	> -2.610	> -2.435	> -2.145	> -1.738		> -1.839	< -1.603	
PSS0007+2417	3.838	20.85	> -3.046	> -2.947	-2.641	> -2.404		-2.444	< -2.058	
PSS1535+2943	3.202	20.65			> -1.580	> -1.468	< -1.131	> -1.547	< -0.928	< -0.789
PSS1535+2943	3.761	20.40	> -2.621	> -2.429	-2.327	-2.020			< -1.197	< 0.062
PSS1715+3809	3.341	21.05			-2.989	< -2.122	< -1.947	-2.807	< -2.006	< -1.607
PSS1802+5616	3.391	20.30			> -1.638	> -1.546		-1.544	< -0.896	< -0.565
PSS1802+5616	3.554	20.50				> -1.821		-1.925	< -1.451	< -0.538
PSS1802+5616	3.762	20.55	> -2.466		> -2.080	> -1.740			< -1.468	
PSS1802+5616	3.811	20.35	> -2.528		-2.447	-2.040		-2.185	< -1.522	
PSS2315+0921	3.219	21.35			> -2.600		< -1.829	> -2.293		< -2.073
PSS2315+0921	3.425	21.10			> -1.809	-1.511		> -1.965	< -1.991	

TABLE 15
RELATIVE ABUNDANCE SUMMARY

Name	z_{abs}	N(HI)	[C/Fe]	[O/Fe]	[Al/Fe]	[Si/Fe]	[Cr/Fe]	[Ni/Fe]	[Zn/Fe]
PSS0007+2417[a]	3.496	21.10			> -0.520	$+0.238$	$< +1.247$		$< +0.441$
PSS0007+2417	3.705	20.55							
PSS0007+2417	3.838	20.85	> -0.602	> -0.503	-0.197	$> +0.040$		$< +0.386$	
PSS1535+2943	3.202	20.65							
PSS1535+2943[b]	3.761	20.40	> -0.294	> -0.102		$+0.307$		$< +1.130$	$< +2.389$
PSS1715+3809	3.341	21.05			-0.182	$< +0.685$	$< +0.860$	$< +0.801$	$< +1.200$
PSS1802+5616	3.391	20.30			> -0.094	> -0.002		$< +0.648$	$< +0.979$
PSS1802+5616	3.554	20.50				$> +0.104$		$< +0.474$	$< +1.387$
PSS1802+5616	3.762	20.55							
PSS1802+5616	3.811	20.35	> -0.343		-0.262	$+0.145$		$< +0.663$	
PSS2315+0921	3.219	21.35							
PSS2315+0921	3.425	21.10							

[a] Ni is serving as a proxy for Fe
[b] Al is serving as a proxy for Fe

4. SUMMARY

Tables 14 and 15 present a summary of the absolute and relative abundances of the 12 damped Lyα systems in this dataset. In Table 15, where we present abundances relative to Fe, we have considered Ni or Al as a proxy for Fe in a few cases as noted.

We have presented ionic column density measurements for the 12 new damped Lyα systems drawn from the PSS survey. We have measured metal-line column densities with the apparent optical depth method and N(HI) values through qualitative fits to the Lyα profiles. All of the data has been reduced and analysed with the same techniques. Visit `http://www.ucolick.org/~xavier/ESI` for tables, figures and updated measurements, `http://www.astro.caltech.edu/~george/z4.qsos` for information on the PSS quasars, and `http://kingpin.ucsd.edu/~hiresdla/` for the HIRES damped Lyα abundance database and relevant atomic data.

The authors wish to recognize and acknowledge the very significant cultural role and reverence that the summit of Mauna Kea has always had within the indigenous Hawaiian community. We are most fortunate to have the opportunity to conduct observations from this mountain. We acknowledge the Keck support staff for their efforts in performing these observations.

REFERENCES

Castro, S., Djorgovski, S.G., & de Carvalho, R. 2003, ApJS, submitted
Djorgovski, S.G., Gal, R.R., Odewahn, S.C., de Carvalho, R.R., Brunner, R., Longo, G., & Scaramella, R. 1998, in "Wide Field Surveys in Cosmology", eds. S. Colombi & Y. Mellier, Gif sur Yvette: Editions Frontieères, p. 89 (astro-ph/9809187)
Djorgovski, S.G., Mahabal, A., Brunner, R., Gal, R., Castro, S., de Carvalho, R., & Odewahn, S.C. 2001, in: Virtual Observatories of the Future, eds. R. Brunner, S.G. Djorgovski & A. Szalay, ASPCS, 225, 52 (astro-ph/0012453)
Grevesse, N., Noels, A., & Sauval, A.J. 1996, In: Cosmic Abundances, S. Holt and G. Sonneborn (eds.), ASPCS, V. 99, (BookCrafters: San Fransisco), p. 117
Holweger, H. 2001, in Solar and Galactic Composition, ed. R.F. Wimmer-Schweingruber, (Berlin: Springer), 23
Kennefick, J.D., de Carvalho, R., Djorgovski, S.G., Wilber, M., Dickson, E., Weir, N., Fayyad, U., & Roden, J. 1995a, AJ, 110, 78
Kennefick, J.D., Djorgovski, S.G., & de Carvalho, R. 1995b, AJ, 110, 2553
Prochaska, J.X., Gawiser, E., & Wolfe, A.M. 2001, ApJ, 552, 99 (PGW01)
Prochaska, J.X., Gawiser, E., Wolfe, A.M., Cooke, J., & Gelino, D. 2003, ApJS, in press (P03)
Prochaska, J. X. & Wolfe, A. M. 1997, ApJ, 486, 73
Savage, B. D. and Sembach, K. R. 1991, ApJ, 379, 245
Sheinis, A.I., Miller, J., Bigelow, B., Bolte, M., Epps, H., Kibrick, R., Radovan, M., & Sutin, B. 2002, PASP, 114, 851
Storrie-Lombardi, L.J. & Wolfe, A.M. 2000, ApJ, 543, 552